Tailoring Porosity in Carbon Nanospheres for Lithium–Sulfur Battery Cathodes

Guang He,[†] Scott Evers,[†] Xiao Liang,[†] Marine Cuisinier,[†] Arnd Garsuch,[‡] and Linda F. Nazar*[,†]

[†]Department of Chemistry and the Waterloo Institute for Nanotechnology, University of Waterloo, 200 University Avenue West, Waterloo, Ontario N2L 3G1, Canada and [‡]BASF SE, GCN/EE - M311, 67056 Ludwigshafen, Germany

ABSTRACT Porous hollow carbon spheres with different tailored pore structures have been designed as conducting frameworks for lithium–sulfur battery cathode materials that exhibit stable cycling capacity. By deliberately creating shell porosity and utilizing the interior void volume of the carbon spheres, sufficient space for sulfur storage as well as electrolyte pathways is guaranteed. The effect of different approaches to develop shell porosity is examined and compared in this study. The most highly optimized sulfur–porous carbon nanosphere composite, created using pore-formers to tailor shell porosity, exhibits excellent cycling performance and rate capability. Sulfur is primarily confined in 4–5 nm mesopores in the carbon shell and inner lining of the shells, which is beneficial for enhancing charge transfer and accommodating volume expansion of sulfur during redox cycling. Little capacity degradation (~0.1% /cycle) is observed over 100 cycles for the optimized material.

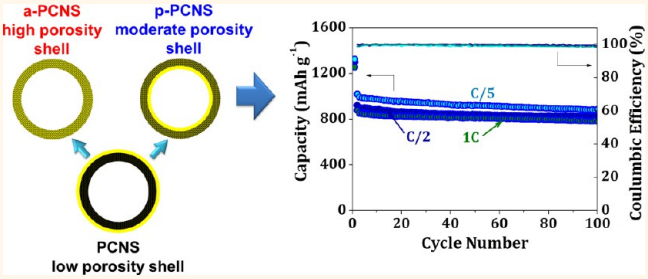

KEYWORDS: lithium–sulfur battery · sulfur cathode · hollow nanospheres · mesoporous carbon

Lithium-ion batteries are being increasingly used for large-scale energy storage systems, driven by the growth of markets such as electric vehicles and large-scale energy storage systems.[1,2] Their practical use in these new applications is still problematic, however, as long as the achievable energy density of Li-ion batteries is limited to their current forms. In this regard, following 20 years of development, intercalation-based cathode materials have almost approached their theoretical energy density limit.[3−5] It is anticipated that breakthroughs will probably come from chemical transformation or conversion chemistry, similar to the evolution of anodes from carbonaceous materials that function on the basis of intercalation chemistry, to conversion chemistry based on metal oxides or lithium alloys.[6] Among various "chemical transformation"-based cathodes, sulfur is a particularly attractive candidate owing to its high theoretical capacity (1675 mAh g^{-1}),[7] low safety concerns/environmental footprint, very high natural abundance, and competitive cost.[8,9] Practically speaking, Li–S batteries have been shown to be capable of energy storage several times greater than conventional large-scale Li-ion cells.[10] Much effort has been expended to date in order to better develop these cells in the past few years, and a deeper understanding of their electrochemistry has resulted in substantial advances, as recently summarized.[11] The fact that sulfur is an outstanding insulator and low-temperature melting solid has necessitated the development of many clever routes to encapsulate the element in conductive carbons using melt-diffusion and vapor infusion methods along with other synthetic approaches as discussed below. Mechanical stability is also problematic, owing to the difference in density between sulfur (2.07 g cm^{-3}) and its redox end member, Li_2S (1.67 g cm^{-3}). The 20% density difference results in ~80% volume expansion on lithiation, and potential loss of electrical contact and degradation of capacity on cycling. To a large degree, this can be solved by designing in extra space in a host framework to accommodate for expansion, as illustrated by a few reports.[12,13]

Several other critical issues still remain, however, as unsolved problems that need to be resolved to achieve future commercialization. Among these, one challenge lies

* Address correspondence to lfnazar@uwaterloo.ca.

Received for review August 25, 2013 and accepted November 9, 2013.

Published online November 14, 2013
10.1021/nn404439r

in achieving high practical sulfur content in the positive electrode while maintaining good electrochemical performance. This relates to the issue of volume expansion, since very high pore volumes, which are difficult to attain in mesoporous carbons, are needed to sustain both redox expansion and >80% sulfur content (*i.e.*, upward of 4 cm^3 g^{-1}). A second primary challenge lies in the often poor capacity retention on cycling because of the shuttle phenomenon due to the soluble intermediate species (polysulfide anions, Li_2S_x, $4 \leq x \leq 8$) formed at the cathode during charge and discharge. If not "contained", the dissolved Li polysulfides diffuse out of the cathode into the electrolyte, where they will ultimately be reduced to form thick layers of Li_2S either on the surface of the metallic Li negative electrode (by contact) or on the outer surface of the cathode on the subsequent discharge cycle. Both mechanisms are responsible for degradative capacity loss and an increase in surface impedance, owing to the insulating nature of Li_2S and its low ion conductivity.[14] Although deposition on the negative electrode surface can be mitigated by employing $LiNO_3$ in the electrolyte as a passivating agent (or ion-conductive membranes) for the Li negative electrode,[15] the buildup of impregnable layers on the cathode is more difficult to address without attention to the rational design of porous materials. In response to this, a large variety of novel carbon architectures, such as micro/mesoporous carbons, have been utilized as a framework for sulfur, which suppress the shuttle by trapping the soluble polysulfide species in the pores, as well as improving the electronic conductivity of the cathode.[16−22] Other approaches have focused on sulfur powder encapsulated with conductive polymers such as polyaniline, polythiophene, and PEDOT to inhibit dissolution, taking advantage of their morphology and electrochemical stability to produce stable composites that yield capacities around 650−800 mAh g^{-1} after 50 cycles. Some studies were conducted at low (100 mA g^{-1}) current rates,[23−27] and it is noteworthy that these polymers are unlikely to be in their conductive state at Li−S cell potentials. Most recently, polyvinylpyrrolidone-encapsulated hollow sulfur nanospheres have demonstrated capacity retention of 78% over 300 cycles at current density rates of C/5 (equivalent to lithium full discharge in 5 h).[28] Graphene−sulfur composites have also been employed, with good success.[29−32]

Alternatively, it has also been proposed to contain sulfur in hollow carbon nanoparticles, as a method of targeted design of porous materials that could—in principle—allow for higher sulfur content while still retaining the benefits of a porous carbon shell that inhibits polysulfide dissolution.[33−35] Such mesoporous hollow carbon capsules might offer advantages over other porous carbon materials, presenting a very attractive conducting matrix for encapsulating and sequestering sulfur on the nanoscale within their interiors. This might allow for higher sulfur content, accommodating volume changes, optimizing electrolyte uptake, and permitting manufacture on a large scale. This has become an increasingly topical area. Important questions concern how to create homogeneously sized, intact spheres in order to facilitate uniform redox of the active sulfur mass. Of equal concern is how to design a mesoporous shell structure that allows for maximum uptake of sulfur in the capsules and minimal lithium polysulfide dissolution while maximizing good electrolyte transport into the interior space. Even more importantly, do the hollow nanospheres fill or partially fill with sulfur (namely, what are the driving forces for sulfur impregnation, or does sulfur often simply coat the external surface of the spheres)? Here, we provide a broad view of the possibilities and limitations of porous hollow carbon nanospheres for Li−S battery cathodes using designed approaches to develop both porosity and robust shell properties. The employment of pore-forming agents that can be readily extracted from the shell after formation of the carbon nanospheres was found to be particularly advantageous. Such a design permits deliberate tuning of the pore size, which differs from the approach taken in prior reports of carbon nanospheres and allows the properties to be tailored to optimum advantage.

RESULTS AND DISCUSSION

Porous carbon nanospheres (PCNSs) were synthesized using tetraethoxysilane (TEOS) as the silica precursor and resorcinol/formaldehyde (RF) as the carbon precursor. To further increase and tailor the shell porosity, two routes were chosen: KOH activation of the carbon in the shell, and the incorporation of a cationic ionomer into the shell of the carbon spheres, which acts as a sacrificial pore-former. The discussion below first centers on the PCNS obtained without pore modification, later comparing these to the modified materials.

The process underlying the one-step assembly of the carbon-shell silica sphere is simple. It is well known that both TEOS and RF undergo hydrolysis in the presence of NH_4OH as a catalyst. However, because TEOS hydrolysis proceeds much faster, it yields solid nanosilica particles (formed via the Stoeber process) surrounded with a coordination shell of NH_4^+ ions. These positively charged silica nanospheres strongly interact with the OH^- groups of the RF polymer due to electrostatic attraction. Therefore, a polymer layer forms on the silica surface to give a core−shell structure. After the calcination of the silica/RF composite and subsequent HF etching of the silica core, hollow carbon nanospheres are obtained as the final product. Unlike most of the hollow nanoparticles obtained *via* a conventional hard-template route, this one-step

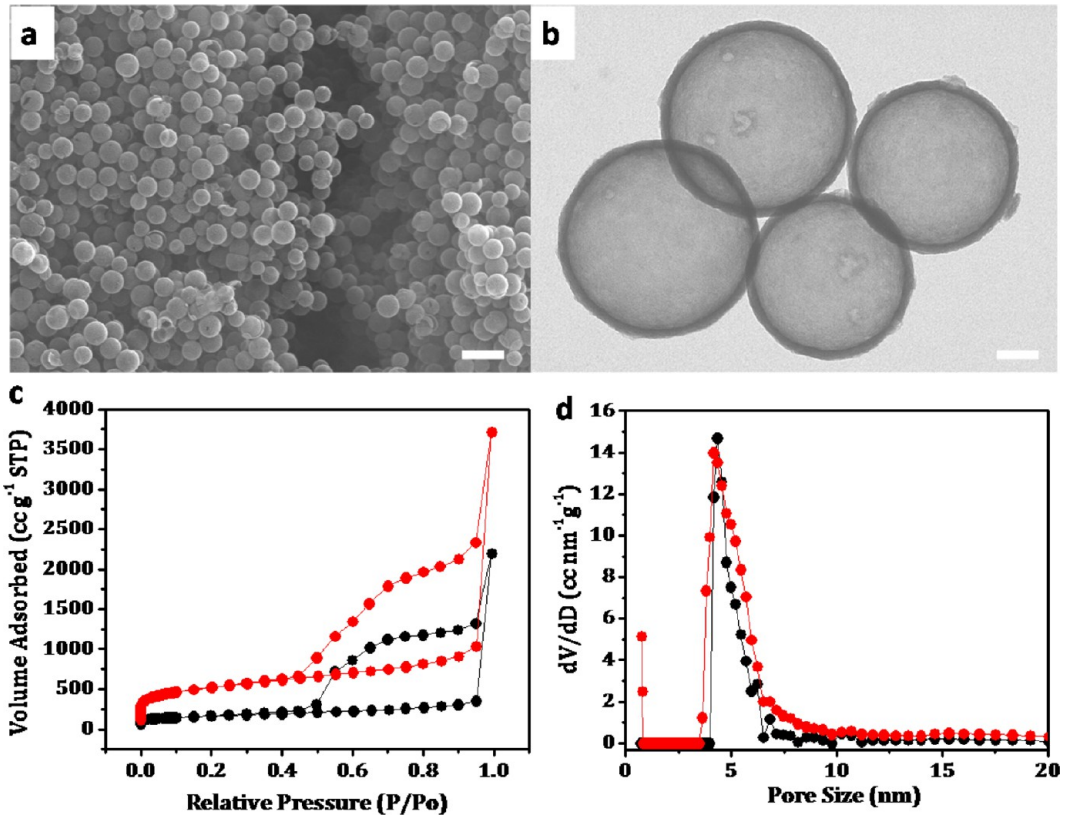

Figure 1. (a) SEM and (b) STEM images showing the uniform PCNSs and (c) N_2 adsorption isotherm and (d) pore size distribution curves (PCNS in black and a-PCNS in red). Scale bars: 400 nm (a) and 50 nm (b).

method is much easier and very time efficient. More importantly, the hollow carbon spheres produced in this way show a very uniform morphology and robust shell structure compared to two-step procedures. Figure 1a demonstrates that the product consists of a homogeneous distribution of spherical carbon nanoparticles, which exhibit only a tiny fraction of broken shells. The hollow structure of the spheres is confirmed by TEM (Figure 1b). The mean particle size of the spheres obtained from both SEM and TEM is ~200 nm, with a shell thickness of 10−12 nm. The porosity of this carbon shell (not evident in the TEM image) measured by N_2 adsorption analysis indicates a low specific surface area of 550 $m^2\ g^{-1}$, a total pore volume of 3.3 $cm^3\ g^{-1}$ (Figure 1c, black curve, P/P_o = 0.999), and a narrow pore size distribution at ~5 nm calculated by the quenched solid density functional theory (QSDFT) method (Figure 1d, black curve). It is reported that solid carbon nanospheres (mean particle size 520 nm) synthesized *via* a similar path have a comparable surface area, but a much smaller total pore volume (less than 0.3 $cm^3\ g^{-1}$).[36] The large total pore volume of the PCNS arises from the textural porosity between the nanospheres, as well as the internal hollow space of each single particle. The real pore volume of the shells estimated at $P/P_o = 0.8$[37] (a pore size of <13 nm, which is just a little less than the thickness of the shells) is ~0.4 $cm^3\ g^{-1}$, as determined from the adsorption branch. The PCNS-70 C/S composite was fabricated by a melt-diffusion process at 155 °C to achieve a 70 wt % sulfur content. This nanocomposite exhibits darker contrast in the shells than those of PCNS in the TEM images (Figure 2a), a sign of sulfur impregnation in the shell pores with possible inhomogeneous deposition of sulfur on the outside of the spheres. The corresponding elemental maps of the particles demonstrate a good distribution of sulfur (Figure 2b and c). The line scan analysis indicates that sulfur fills the mesopores of the shell (and possibly resides on the outer surface) rather than diffusing into the internal void (Figure 2d).

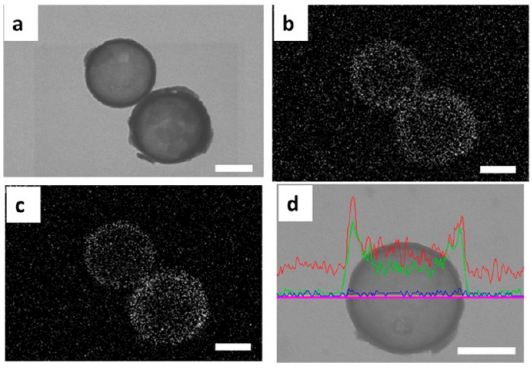

Figure 2. (a) STEM image of PCNS-70, elemental maps of (b) sulfur and (c) carbon, and line scan analysis of a single PCNS-70 particle (red-carbon, green-sulfur). All scale bars: 100 nm.

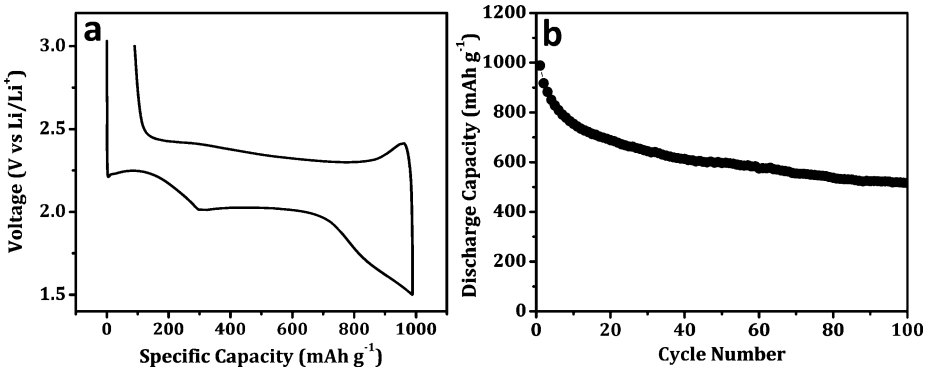

Figure 3. (a) Initial voltage-capacity profile and (b) cycling performance of the PCNS-70 sulfur cathode at a C rate (1675 mA g^{-1}).

The PCNS-70 cathode was evaluated in a coin cell with metallic lithium as the anode and 1 M bis-(trifluoromethanesulfonyl)imide lithium in 1,3-dioxolane + 1,2-dimethoxyethane (2 wt % $LiNO_3$) as the electrolyte. At a 1C rate (1675 mA g^{-1}), the cell exhibits a discharge capacity of ~1000 mAh g^{-1} (Figure 3a). The two plateaus at 2.2 and 2.0 V represent the two steps of sulfur reduction at the cathode, as reported by many other groups. The slope below 1.7 V is not always observed. Previous reports indicate it is probably caused by the partial reduction of $LiNO_3$ during discharge,[38] which also explains the irreversible capacity (90 mAh g^{-1}) on the first cycle. Upon further cycling, this slope gradually disappears. The cell capacity drops significantly by ~35% over the first 20 cycles and then becomes relatively stable over the remaining 80 cycles. After 100 cycles, only about 52% of the initial capacity is retained, as shown in Figure 3b.

We believe the capacity fading is associated with the lack of sufficient porosity in the shell of PCNSs, which in this case is solely derived from the pyrolysis of the RF polymer. Although the shell thickness is ~12 nm (see Figure 1b), the lack of sufficient porosity (the structural pore volume is 0.4 cm^3 g^{-1}, with a surface area similar to solid carbon nanospheres as discussed above) greatly constrains the amount of sulfur that can be incorporated in the porous shell. Thus, most of the sulfur must form a thin layer on the external surface of the spheres (see above for discussion of TEM elemental mapping), because 70 wt % sulfur cannot be contained in a pore volume of 0.4 cm^3 g^{-1}. However, this fraction of sulfur can easily be accommodated on the surface of the porous carbon hollow nanospheres owing to their very high surface area. This could possibly play a factor in other reports where shell porosity is low. As a result, the close contact between sulfur and carbon allows a high discharge capacity at high current rate, but the exterior sulfur layer without pore/shell protection is readily dissolved in the electrolyte upon reduction to polysulfides and is lost, which leads to the capacity fading on cycling, as shown in Figure 3b. Thus it is critical to create more porosity in the shells to allow more sulfur to be imbibed within the spheres. Two methods were utilized to achieve this goal.

Activated-Carbon PCNS. First, the pore volume was increased by KOH activation, a well-established approach to produce microporosity in carbonaceous materials.[39] The N_2 adsorption isotherm of the activated-PCNS (a-PCNS) exhibits an analogous shape to that of the as-prepared PCNS. However, the Brunauer–Emmett–Teller (BET) surface area and total pore volume of a-PCNS are significantly increased to 1800 m^2 g^{-1} and 5.4 cm^3 g^{-1}, respectively (Figure 1c, red curve). The pore size distribution curves of PNCS and a-PCNS are almost identical except for the addition of abundant microporosity in the latter, implying that the extra surface area and pore volume after activation are derived mainly from the micropores, while the original mesopores are maintained (Figure 1d, red curve). The structural pore volume calculated at P/P_o = 0.8 is 1.4 cm^3 g^{-1}, more than 3 times higher than for PCNS, which also confirms the increased porosity of the carbon shells.

Due to the aggressive etching process by KOH, defects are introduced into the a-PCNS nanospheres that result in deformity of the carbon shell and the presence of caved-in structures (Figure 4a). Even with 70 wt % of sulfur in the material, the concave surface of the a-PCNS-70 composite is still evident in the TEM image in Figure 4b. The successful impregnation of sulfur into the hollow structure of the carbon particles is confirmed by the line scan, which shows a very homogeneous sulfur distribution in the carbon spheres (Figure 4c). The first discharge capacity of this sample is ~1300 mAh g^{-1} at a 1C rate, about 78% of the theoretical capacity (Figure 5a, black curve). Even considering the initial contribution from reduction of $LiNO_3$, the real discharge capacity of the active material sulfur is still about 1200 mAh g^{-1}. This high initial capacity at such a high current rate suggests the cathode is very favorable for both charge and mass transfer and also provides evidence of the homogeneous distribution of sulfur in the hollow sphere

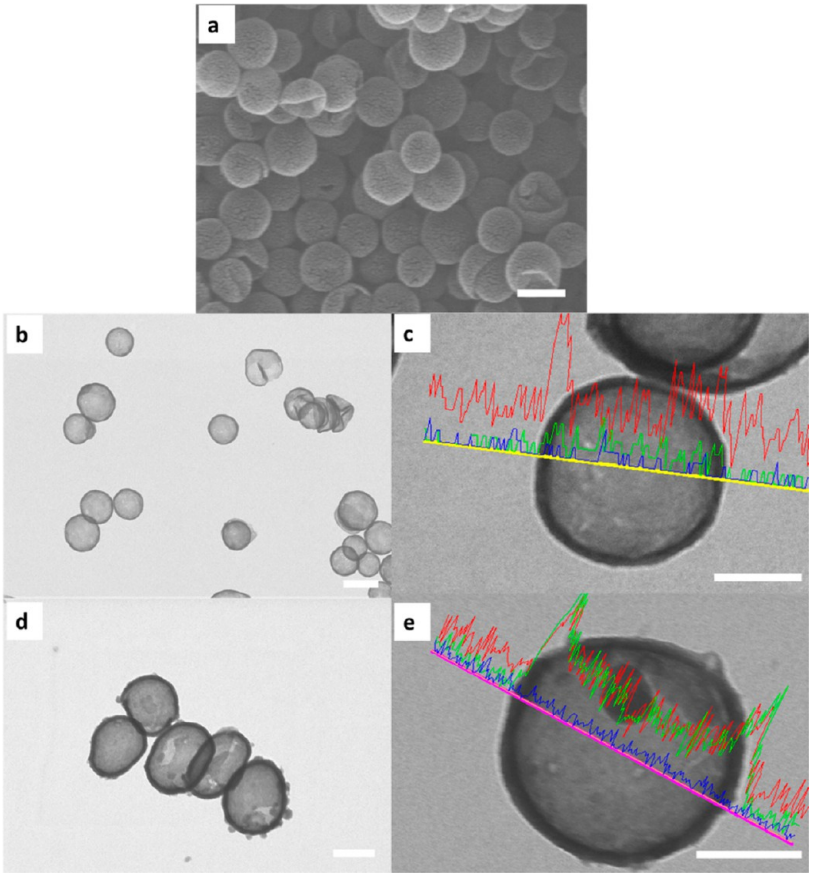

Figure 4. (a) SEM image of a-PCNS, (b) TEM image and (c) line scan analysis of a-PCNS-70, and (d) TEM image and (e) line scan analysis of a-PCNS-80 (red-carbon, green-sulfur). Scale bars: 200 nm for a, b, d, and 100 nm for c, e.

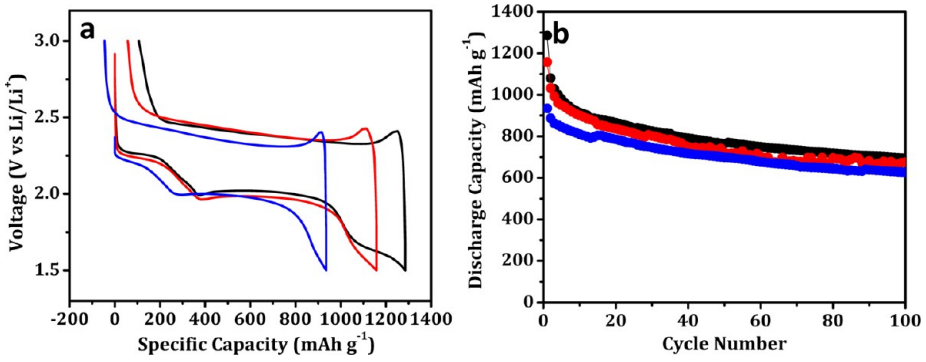

Figure 5. (a) Initial voltage-capacity profile and (b) cycling performance of the three C/S cathodes a-PCNS-70 (black), a-PCNS-75 (red) and a-PCNS-80 (blue) at C rate (1675 mA g^{-1}).

framework. By increasing the sulfur ratios to 75 and 80 wt % in the C/S, the initial capacities of the two samples decrease to 1150 and 940 mAh g^{-1}, respectively. Theoretically, the extremely large total pore volume (5.4 cm^3 g^{-1}) of a-PCNS can contain as much as 88 wt % sulfur in the C/S considering full electrode conversion (ρ_S = 2.0 g cm^{-3}, ρ_{Li2S} = 1.6 g cm^{-3}) between S and Li_2S. However, the existence of textural volume indicates the real available sulfur loading ratio is undoubtedly less. Moreover, impregnation of significant sulfur on the *interior* surface of the carbon nanospheres is unlikely because as more and more sulfur is impregnated into the pores and the internal surface, the pathway is gradually blocked. Thus, the hollow space of the spheres is actually not well utilized for sulfur loading. This conclusion is supported by the TEM image of a-PCNS-80 in Figure 4d, which does not show any obvious internal sulfur contribution compared to a-PCNS-70. The line scan of a single a-PCNS-80 particle shown in Figure 4e displays similar results to the PCNS-70 sample, where sulfur fills the pores of the shell. These results obtained from the TEM and EDAX line scans are consistent with the relatively low initial capacity of the a-PCNS-80 among the three samples.

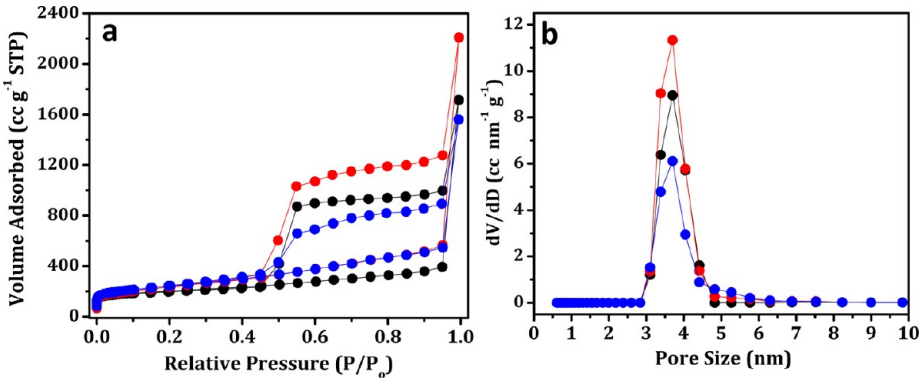

Figure 6. (a) N_2 adsorption isotherms of three p-PCNS and (b) the corresponding pore size distribution curves. (black-low, red-medium and blue-high).

In spite of this, a discharge capacity of 940 mAh g^{-1} at a 1C rate for a sulfur cathode with 80 wt % active material is still unusual for mesoporous sulfur electrodes because of the fact that very few examples of mesoporous carbon have been reported with a high pore volume (*i.e.*, > 3.5 cm^3 g^{-1}) and 80 wt % sulfur. The three C/S cathodes exhibit a similar cycling trend, as shown in Figure 5b. After 100 cycles, the capacities of the three cathodes are 700, 680, and 630 mAh g^{-1}, which are 54%, 60%, and 68% of the initial discharge capacities, respectively. By comparison with the PCNS-70 sample, both the initial and remaining capacities obtained with the activated carbon spheres are higher, nonetheless, showing the significant progress obtained by increasing the porosity of the shells. The fabrication of spherical carbon with a "trimodal" nanostructure (uniform micropores and mesopores and very small (200 nm) particle size) with a superior large pore volume is a significant step for porous materials chemistry as well.

However, the capacity retention of less than 70% is too low for practical applications of a Li−S battery. There are two possible reasons for the relatively rapid fading. First, the activation process partially destroys the robust thin shells of the spheres, as evident from their deformity. Maintaining an intact spherical shell is one of the key factors for good electrochemical performance of the cathodes, as it provides a physical barrier for the soluble polysulfide species. Second, for those carbon nanospheres with complete shells, too much additional porosity in the shell produced by the KOH activation process may enable solvated polysulfide anions to diffuse out from the interior. Accordingly, the abundant porosity can be a disadvantage of the a-PCNS with respect to polysulfide retention. This finding suggests that a framework with larger pore volume and surface area does not necessarily lead to better electrochemistry for sulfur cathodes. Even though the ion conductivity and rate capability of the cathode are enhanced in a very porous framework, the porosity facilitates the transfer of both lithium ions and polysulfide anions, which causes reduced cycling stability.

Tailored-Pore PCNS. In order to increase the porosity in the carbon shell in a controlled fashion that is less destructive than KOH activation, a cationic surfactant was introduced into the precursor, following an adaptation of a report by Bruno *et al.* that used cetyltrimethylammonium bromide to produce carbon mesogels from resorcinol−formaldehyde blends.[40] We instead chose polyDADMAC (poly(diallyldimethylammonium chloride)), a cationic homopolymer, as a pore-forming agent owing to its large hydrodynamic radius.[41] To create these "p-PCNSs", the resorcinol and formaldehyde (RF) were mixed with a polyDADMAC solution and added as one solution to the TEOS instead of separately. This was carried out to ensure the complete incorporation of polyDADMAC within the RF polymer. The pore-former content controls the shell porosity and thickness; the ~20 nm thick shells (see below) maintain robust; while the 4 nm pores are large enough to enable the PCNSs to be impregnated with sulfur by melt-diffusion and readily permit ingress of electrolyte. Three different fractions of added polyDADMAC were examined in order to fully optimize the porosity in the carbon shell to allow for sulfur impregnation and facile lithium ion transport while retaining soluble polysulfides. These are defined as materials with a high concentration of pore-former (p-PCNS-H; 480 μL of polyDADMAC, see Methods) and low and intermediate concentrations of pore-former (p-PCNS-L and -M; 180 and 240 μL of polyDADMAC, respectively).

The physical properties of the three p-PCNS materials were examined by nitrogen adsorption experiments. Shown in Figure 6a are the BET isotherms. All three materials have a typical type IV hysteresis that signifies mesoporosity created by the polyDADMAC incorporation and its subsequent removal. The pore size distribution is shown in Figure 6b. It is readily apparent that more polyDADMAC creates more porosity in the shell, but too much polyDADMAC actually decreases the relative porosity. A summary of the physical properties of each material is given in Table 1, from which several conclusions can be drawn.

There is less porosity with low polyDADMAC fractions, but at high concentrations the porosity sharply declines. As the polyDADMAC concentration increases, the surface area increases, but the pore volume finds a maximum at intermediate concentration. It significantly decreases at high concentration. The pore size remains constant at all of concentrations used since it is directly related to the size and conformation of polyDADMAC embedded in the RF polymer based on its compressed hydrodynamic radius. The nitrogen adsorption measurements show that an optimum material (p-PCNS-M) is prepared by adding an intermediate amount of polyDADMAC. Prior to sulfur impregnation the p-PCNS-M has high surface area (824 $m^2\ g^{-1}$) and total pore volume (3.42 $cm^3\ g^{-1}$) determined from BET measurements, with a narrow pore size distribution centered at 4.3 nm. As mentioned above, the majority of the pore volume is due to the large void volume (interior of the spheres) based on its high relative pressure response. It can be estimated from QSDFT (or from the intermediate pressure response at $P/P_o = 0.8$) that ~1.1−1.6 $cm^3\ g^{-1}$ arises from the shell alone. The trends in surface area and pore volume are easily corroborated by examining the material's morphology by SEM analysis. The morphology of the samples is shown in Figure 7. At low and medium polyDADMAC concentrations (Figure 7a and b) the sphere's morphology and size are homogeneous and almost devoid of any broken shells. At higher concentrations (Figure 7c) the walls of the spheres become fragile and a larger number of spheres exhibit broken shells. This decreases the pore volume of the material, but the surface area increases because of the new surfaces created by broken shells. The wall thickness of the optimum surfactant-modified carbon material (p-PCNS-M) shown in Figure 7b is estimated to be 20−25 nm, which is greater than of the initial PCNS and further adds to the mechanical stability of the spheres.

TABLE 1. Physical Properties of the Three p-PCNS Nanospheres with Respect to the Molar Ratio of TEOS, Resorcinol, and Pore Former, Poly(diallyldimethylammonium chloride)

	surface area ($m^2\ g^{-1}$)	pore volume ($cm^3\ g^{-1}$)	pore size (nm)
p-PCNS-L (low)[a]	763	2.65	4.3
p-PCNS-M (int)[b]	956	3.42	4.3
p-PCNS-H (high)[c]	1055	2.41	4.3

[a] Molar ratio: 1:0.48:6.8 × 10^{-3}. [b] Molar ratio: 1:0.48:9.0 × 10^{-3}. [c] Molar ratio: 1:0.48:1.8 × 10^{-2}.

The robustness of this material and its porosity are also demonstrated by incorporation of sulfur into the nanospheres. As in the previous examples, the sulfur content of the p-PCNS-M/S determined by thermogravimetric analysis (TGA; Figure 8a; inset) was ~70 wt % as targeted. We note that the pore volume of the shell (~1.1−1.6 $cm^3\ g^{-1}$, *vide infra*) can probably contain all of the sulfur, although this is a rough estimate because that value is not accurately known. The TGA curve shows that the sulfur mass is lost in two distinct temperature regions. Below 280 °C, the loss of 58 wt % sulfur is attributed to bulk sulfur that is infiltrated in the core of the p-PCNSs and the mesopores of the shell. Above 280 °C, an additional 10 wt % sulfur evolves with weight loss continuing to 420 °C. This high-temperature sulfur is presumably highly confined in the interior of the structure (*i.e.*, on the inner lining of the shell) based on the higher temperature of volatilization. The TEM image and corresponding EDX line scan of a representative p-PCNS-M particle with a diameter of ~220 nm and a shell thickness of ~20−25 nm and 70 wt % sulfur is shown in Figure 8a (p-PCNS-M-70).

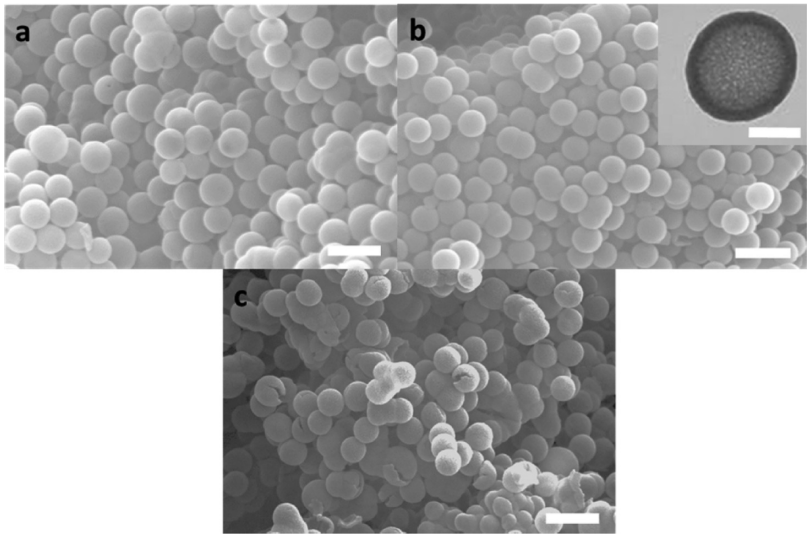

Figure 7. (a) SEM images of the three p-PCNSs with different concentrations of pore-former (p-PCNS-L; p-PCNS-M and p-PCNS-H) as described in the text and in Table 1. The polyDADMAC content increases from (a) to (c), indicating that a surfeit of pore-former destroys the shell intactness. Scale bars: 500 nm for (a), (b), and (c) and 100 nm for the inset TEM in (b).

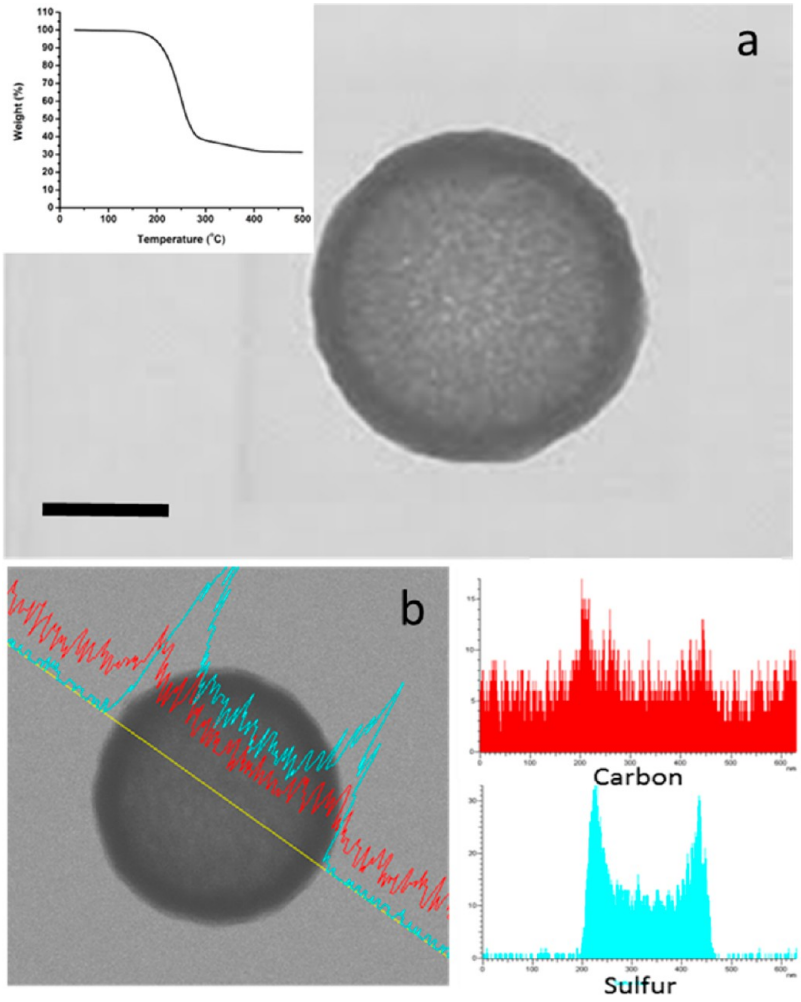

Figure 8. (a) Representative STEM image of p-PCNS-M-70 (scale bar 100 nm), inset shows TGA curve obtained for the material; b) STEM image of p-PCNS-M-70 (left) and EDX line scan (right) showing the carbon and sulfur distribution.[47]

The morphology of the particle remains intact on sulfur impregnation, and the diameter and shell thickness remained constant as well. This indicates a discernibly different sulfur profile than the sulfur-imbibed PCNS and a-PCNS materials, namely, a higher S/C ratio throughout the shell and the inner lining where the sulfur is confined, and no sulfur contribution from the exterior. The sulfur contribution from the interior, suggested by the TGA data above, is echoed in the line scan (Figure 8b). The other two p-PCNS materials (p-PCNS-H and p-PCNS-L) were also imbibed with 70 wt % sulfur similar to that of p-PCNS-M, and their electrochemical properties were studied using the same protocol as described above.

All materials show the two plateau discharge profile typical of a Li−S battery (Figure 9a, inset) with high concentrations of pore-former (p-PCNS-H-70) delivering the highest initial discharge capacity of 832 mAh g^{-1}. Low and medium concentrations of pore-former (p-PCNS-L and -M) resulted in sulfur-imbibed electrodes with slightly lower discharge capacities of 680 and 671 mAh g^{-1}, respectively. The P-PCNS-L and -H derived materials both experience increased polarization at the 100th cycle (not shown) with similar capacities, likely owing to polysulfide reduction on the cathode surface, which would produce an insulating layer of Li_2S-like material. The effective confinement of polysulfides within the interior of the spheres limits high-impedance surface layers from forming on the exterior and extends cycle life. The effectiveness of the materials is evident upon long-term cycling, shown in Figure 9a. The p-PCNS-H-70 material displays significant capacity fading over 100 cycles despite exhibiting the highest initial discharge capacity. The broken spheres of this material allow greater initial reduction of sulfur due to the fact that more sulfur is accessible. However, there is no confinement of sulfur in the spheres to stabilize capacity and limit polysulfide dissolution. The material prepared with a low surfactant concentration, p-PCNS-L-70, exhibits completely intact spheres, but a lower pore volume and less porosity in the carbon shells. This lack of porosity severely limits lithium-ion diffusion and increases sulfur inaccessibility in the spheres.

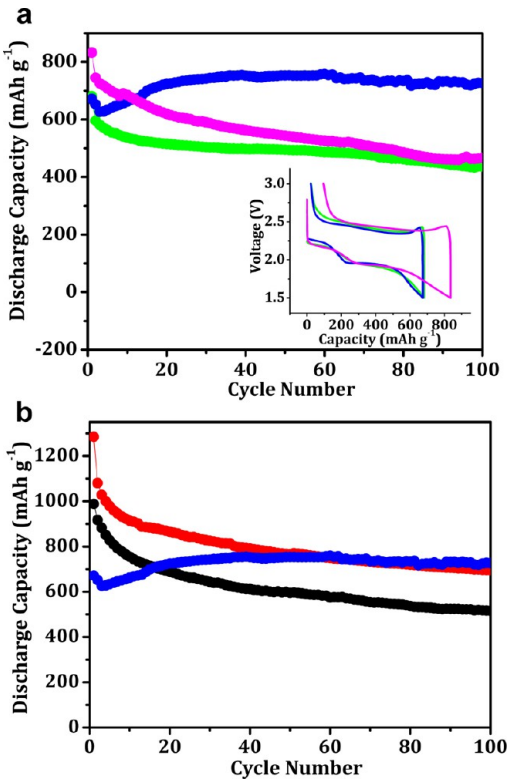

Figure 9. (a) Effect of surfactant content in the shell on the cycling performance of the three p-PCNS-70 at a C rate (1675 mA g^{-1}) for p-PCNS-L-70 (green), p-PCNS-M-70 (blue), and p-PCNS-H-70 (pink), where L, M, and H refer to the concentrations of polyDADMAC pore-former used in the preparation of the p-PCNS (see Table 1). Inset shows the initial voltage–capacity profile. (b) Comparison of cycling performance at a C rate (1675 mA g^{-1}) for the simple, activated-porous, and polyDADMAC-porous PCNSs at a sulfur content of 70 wt %: PCNS-70 (black), a-PCNS-70 (red), and p-PCNS-70 (blue).

The capacity fades quickly initially over the first 20 cycles due to sulfur that is not confined in the spheres, stabilizing at around 500 mAh g^{-1}. The optimal intermediate polyDADMAC concentration, p-PCNS-M-70, in contrast, exhibits excellent capacity retention at a C rate (Figure 9a). Previous reports have detailed high capacity retention in excess of 90% over 100 cycles, but have fallen short at reporting this target above C/2 rates (full discharge in 2 h).[33] The specific discharge capacity experiences a slight fade over the first few cycles that has been reported as an activation step, whereby all of the sulfur in the composite is not initially fully accessible to electrolyte because the pores are filled.[26] The sulfur in the porous carbon shell must first be reduced in order for electrolyte and Li ions to fully penetrate into the inner void of the spheres. After the first few activation cycles, the capacity rises, leveling off to reach about 725 mAh g^{-1} over 100 cycles. The more steady response of the intermediate p-PCNS-M-70 indicates that tuning of the porosity and an intact carbon shell are very important to achieve both high discharge capacity and a stable electrochemical response.

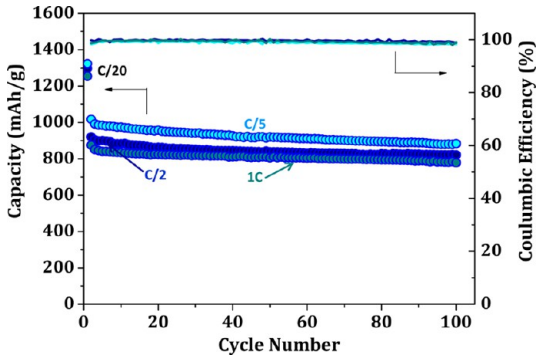

Figure 10. Comparison of the rate capability of optimized electrodes of p-PCNS-M-70 over 100 cycles at rates of 1C (teal), C/2 (navy), and C/5 (cyan).

The different methods used to create shell porosity in the porous hollow carbon spheres are compared in Figure 9b, which shows the cycling stability of PCNS-70, a-PCNS-70, and p-PCNS-M-70, all at 70 wt % sulfur, as a function of cycling index. This comparison reaffirms the trade-off between higher shell porosity and poorer capacity retention. The highest initial capacity (1300 mAh g^{-1}) is obtained with the KOH-activated a-PCNS, which has the most porous shell, presumably owing to the openness of the pore structure, but this material also suffers the greatest degradation in cycling capacity. Lesser initial capacity is observed with the material with no deliberate tailoring of the porosity (PCNS), but about the same capacity fade rate after 20 cycles, which we ascribe to a significant fraction of sulfur on the shell exterior. Although the initial gravimetric capacity is reduced in the tailored pore design of the pore-former p-PCNS, it is well sustained.

Rate testing was therefore performed on p-PCNS-M-70 using an optimized electrode configuration, first using an initial conditioning cycle to allow full egress of electrolyte into the pores. Excellent performance was exhibited (Figure 10), suggesting that reduced polysulfides effectively penetrate the inner void of the spheres and remain in the cathode. A specific capacity of over 875 mAh g^{-1} was exhibited at C rates with a fade rate of 0.1% per cycle, superior to previously reported carbon nanosphere sulfur cathodes.[42−44] At lower current densities, the expected variation of capacity and capacity retention was observed: lower rates provide higher capacity but slightly poorer retention, and the opposite is true for higher rates. For example at a C/5 rate, the cell exhibited an initial discharge capacity of 1015 mAh g^{-1}, which decreased to 880 mAh g^{-1} after 100 cycles (capacity retention of 86.5%). At C/2, the initial capacity was slightly lower (920 mAh g^{-1}), but the retention was higher (89.4%), and at a C rate, a lower initial capacity of 875 mAh g^{-1} with retention of 89.6% (785 mAh g^{-1}) was observed. Overall, this represents a rather small difference in retention for the different current densities, and

a C/2 rate, ideally suited to practical applications, is optimal.

CONCLUSIONS

A scalable approach to precisely tailor the porosity of the shells of hollow carbon nanospheres has been developed using extractable surfactant pore-formers, resulting in optimized carbon spheres that can be easily infiltrated with sulfur. A highly uniform positive Li−S battery electrode material is created where the lithium diffusion length is short and equivalent in all particles. The material prepared with an optimum concentration of pore-former, p-PCNS-M-70, exhibited superior electrochemical results at a high 1C rate and where capacity retention approaches 90% over 100 cycles. More significantly, by comparison to other porous carbon hollow spheres synthesized by other methods, we have achieved a more general understanding of the factors that control sulfur fraction loading in these materials and how porosity tuning affects the electrochemical properties. Thus, with adroit nanostructure design, we demonstrate here that tuned-porosity PCNSs represent a highly viable avenue for Li−S battery technology due to their ease of scale-up as well as their uniformity in size and composition.

METHODS

Synthesis. *PCNS.* Porous carbon nanospheres (PCNSs) were prepared *via* self-assembly from a carbon resin and a silicate source, modifying a previously reported method.[45] Typically, 3.0 mL of an ammonia aqueous solution (28 wt %) was added to a mixture of 10 mL of deionized water and 70 mL of ethanol. After the mixture was stirred for 30 min at 30 °C, tetraethyl orthosilicate (2.8 mL), resorcinol (0.4 g), and formalin (35−37 wt %, 0.56 mL) were added to the solution at intervals of 10 min. The mixture was vigorously stirred for 24 h at 30 °C and maintained at 100 °C for another 24 h in a Teflon-lined autoclave under static conditions. The solid product was then collected by centrifugation and dried at 100 °C for a few hours. Last, it was heated at 750 °C (5 K min^{-1}) for 1 h with the protection of flowing Ar gas to obtain the SiO_2@C composite, and the silica core was dissolved by treating the material in 0.1 M HF overnight.

a-PCNS. To increase the shell porosity, an activated-PCNS (a-PCNS) sample was prepared by KOH activation of the carbon in the shell. Specifically, 200 mg of PCNS powder was first dispersed in 7 M KOH solution by sonication for 1 h and then stirred for 4 h and soaked for another 24 h. The mixture was filtered to obtain the PCNS/KOH composite. After drying in air for 24 h at 65 °C, the composite was heated at 800 °C for 1 h under Ar to yield a-PCNS. Finally, potassium-containing byproducts were removed by washing the sample with both a 1 M HCl solution and deionized water.

p-PCNS. As an alternative route to increase the shell porosity, the polymer surfactant-PCNS (p-PCNS) sample was prepared by the incorporation of a cationic ionomer, poly(diallyldimethylammonium chloride), into the shell of the carbon spheres, which acts as a sacrificial pore-former. The PCNS synthesis was followed as detailed above except that a volume of polyDADMAC (as a 7 wt % aqueous solution) was mixed with the resorcinol and formalin prior to addition to the silica. The volume of polyDADMAC was adjusted to tune the porosity in the shell. Three volumes were used as an additive to the preparation of PCNS (see above): 180, 240, and 480 μL (see Table 1). PolyDADMAC is removed during carbonization at 750 °C under an argon flow to yield pores in the carbon shell.

C/S Composites. C/S composites were prepared by the melt-diffusion approach at 155 °C as previously reported.[46] Vapor phase diffusion was also explored, but this method was determined to be impractical at a large-scale level, in addition to giving rise to a significant fraction of sulfur on the exterior of the spheres. The materials prepared and examined in the electrochemical cells were the following: PCNS-70 (no porosity tuning); a-PCNS-70, a-PCNS-75, a-PCNS-80 (porosity induced *via* KOH, where *a* = activated carbon); p-PCNS-L-70, p-PCNS-M-70, p-PCNS-H-70 (porosity induced *via* polymer surfactant, where p = pore-former and where L, M, and H refer to the concentration of pore-former).

Characterization. Surface area, pore volume, and pore size were determined from nitrogen adsorption and desorption isotherms performed on a Quantachrome Autosorb-1 instrument at 77 K. Before measurement the samples were degassed at 150 °C on a vacuum line. The total pore volumes of carbon and the C/S composites were calculated at a relative pressure of 0.999 (P/P_o). The specific surface area, pore size distribution, and pore volumes were determined by BET theory and the QSDFT model from the desorption branch of the isotherms. Field-emission scanning electron microscopy images were acquired on a LEO 1530 instrument. Scanning transmission electron microscopy (STEM) was carried out on a Hitachi HD-2000 STEM.

Electrochemistry. The C/S cathode materials were slurry-cast from *N,N*-dimethylformamide onto a carbon-coated aluminum or carbon current collector, using an positive electrode formulation of C/S:Super P:Kynar Flex = 80:10:10. A typical electrode loading was 4−5 mg of sulfur/porous carbon nanosphere composite for a 2 cm^2 current collector. The electrolyte was 1 M bis(trifluoromethanesulfonyl)imide lithium in a mixed solvent of 1,2-dimethoxyethane and 1,3-dioxolane (v/v = 1:1), with 2 wt % of $LiNO_3$. Metallic lithium was used as the negative electrode. Cells were cycled in a voltage window between 3.0 and 1.5 V, except for the rate performance experiments, where the window was between 3.0 and 1.8 V.

Conflict of Interest: The authors declare no competing financial interest.

Acknowledgment. This research was supported by the BASF International Scientific Network for Electrochemistry and Batteries. We thank NSERC for generous support *via* a Canada Research Chair to L.F.N. We gratefully acknowledge N. Coombs, University of Toronto, for help with acquisition of the TEM images.

REFERENCES AND NOTES

1. Zaghib, K.; Mauger, A.; Groult, H.; Goodenough, J. B.; Julien, C. M. Advanced Electrodes for High Power Li-ion Battery. *Materials* **2013**, *6*, 1028–1049.
2. Liu, J.; Zhang, J.-G.; Yang, Z.; Lemmon, J. P.; Imhoff, C.; Craff, G. L.; Li, L.; Hu, C.; Xiao, J.; Xia, G.; *et al.* Materials Science and Materials Chemistry for Large Scale Electrochemical Energy Storage: From Transportation to Electrical Grid. *Adv. Funct. Mater.* **2013**, *23*, 929–946.
3. Ellis, B.; Lee, K. T.; Nazar, L. F. Positive Electrode Materials for Li-ion and Li-Batteries. *Chem. Mater.* **2010**, *22*, 691–714.
4. Scrosati, B.; Garche, J. Lithium Batteries: Status, Prospects and Future. *J. Power Sources* **2010**, *195*, 2419–2430.
5. Whittingham, M. S. Lithium Batteries and Cathode Materials. *Chem. Rev.* **2004**, *104*, 4271–4301.
6. Choi, N.-S.; Chen, Z.; Freunberger, S. A.; Ji, X.; Sun, Y.-K.; Amine, K.; Yushin, G.; Nazar, L. F.; Cho, J.; Bruce, P. G. Challenges Facing Lithium Batteries and Electrical Double-Layer Capacitors. *Angew. Chem., Int. Ed.* **2012**, *51*, 9994–10024.

7. Yamin, H.; Peled, E. Electrochemistry of a Nonaqueous Lithium/Sulfur Cell. *J. Power Sources* **1983**, *9*, 281–287.
8. Ji, X.; Nazar, L. F. Advances in Li-S Batteries. *J. Mater. Chem.* **2010**, *20*, 9821–9826.
9. Yang, Y.; Zheng, G. Y.; Cui, Y. Nanostructured Sulfur Cathodes. *Chem. Soc. Rev.* **2013**, *42*, 3018–3032.
10. Bruce, P. G.; Freunberger, S. A.; Hardwick, L. J.; Tarascon, J. M. Li-O_2 and Li-S Batteries with High Energy Storage. *Nat. Mater.* **2012**, *11*, 19–29.
11. Evers, S.; Nazar, L. F. New Approaches for High Energy Density Lithium-Sulfur Battery Cathodes. *Acc. Chem. Res.* **2013**, *46*, 1135–1143.
12. Ji, X.; Lee, K. T.; Nazar, L. F. A Highly Ordered Nanostructured Carbon-Sulphur Cathode for Lithium-Sulphur Batteries. *Nat. Mater.* **2009**, *8*, 500–506.
13. Seh, Z. W.; Li, W.; Cha, J. J.; Zheng, G.; Yang, Y.; McDowell, M. T.; Hsu, P.-C.; Cui, Y. Sulphur TiO_2 Yolk-Shell Nanoarchitecture with Internal Void Space for Long-Cycle Lithium-Sulphur Batteries. *Nat. Commun.* **2013**, *4*, 1331–1336.
14. Xiao, L.; Cao, Y.; Xiao, J.; Schwenzer, B.; Engelhard, M. H.; Saraf, L. V.; Nie, Z.; Exarhos, G. J.; Liu, J. A Soft Approach to Encapsulate Sulfur: Polyaniline Nanotubes for Lithium-Sulfur Batteries with Long Cycle Life. *Adv. Mater.* **2012**, *24*, 1176–1181.
15. Aurbach, D.; Pollak, E.; Elazari, R.; Salitra, G.; Kelley, C. S.; Affinito, J. On the Surface Chemical Aspects of Very High Energy Density, Rechargeable Li-Sulfur Batteries. *J. Electrochem. Soc.* **2009**, *156*, A694–A702.
16. Zhang, B.; Qin, X.; Li, G. R.; Gao, X. P. Enhancement of Long Stability of Sulfur Cathode by Encapsulating Sulfur into Micropores of Carbon Spheres. *Energy Environ. Sci.* **2010**, *3*, 1531–1537.
17. Elazari, R.; Salitra, G.; Garsuch, A.; Panchenko, A.; Aurbach, D. Sulfur-Impregnated Activated Carbon Fiber Cloth as a Binder-Free Cathode for Rechargeable Li-S Batteries. *Adv. Mater.* **2011**, *23*, 5641–5644.
18. Liang, C.; Dudney, N. J.; Howe, J. Y. Hierarchically Structured Sulfur/Carbon Nanocomposite Material for High-Energy Lithium Battery. *Chem. Mater.* **2009**, *21*, 4724–4730.
19. He, G.; Ji, X.; Nazar, L. High "C" Rate Li-S Cathodes: Sulfur Imbibed Bimodal Porous Carbons. *Energy Environ. Sci.* **2011**, *4*, 2878–2883.
20. Chen, S.-R.; Zhai, Y.-P.; Xu, G.-L.; Jiang, Y.-X.; Zhao, D.-Y.; Li, J.-T.; Huang, L.; Sun, S.-G. Ordered Mesoporous Carbon/Sulfur Nanocomposite of High Performance as Cathode for Lithium-Sulfur Battery. *Electrochim. Acta* **2011**, *56*, 9549–9555.
21. Schuster, J.; He, G.; Mandlmeier, B.; Yim, T.; Lee, K. T.; Bein, T.; Nazar, L. F. Spherical Ordered Mesoporous Carbon Nanoparticles with High Porosity for Lithium-Sulfur Batteries. *Angew. Chem., Int. Ed.* **2012**, *51*, 3591–3595.
22. Zheng, G.; Yang, Y.; Cha, J. J.; Hong, S. S.; Cui, Y. Hollow Carbon Nanofiber-Encapsulated Sulfur Cathode for High Specific Capacity Rechargeable Lithium Batteries. *Nano Lett.* **2011**, *11*, 4462–4467.
23. Qiu, L.; Zhang, S.; Zhang, L.; Sun, M.; Wang, W. Preparation and Enhanced Electrochemical Properties of Nano-Sulfur/Poly(pyrrole-co-aniline) Cathode Material for Lithium/Sulfur Batteries. *Electrochim. Acta* **2010**, *55*, 4632–4636.
24. Liang, X.; Wen, Z.; Liu, Y.; Wang, X.; Zhang, H.; Wu, M.; Huang, L. Preparation and Characterization of Sulfur-Polypyrrole Composites with Controlled Morphology as High Capacity Cathode for Lithium Batteries. *Solid State Ionics* **2011**, *192*, 347–350.
25. Liang, X.; Liu, Y.; Wen, Z.; Huang, L.; Wang, X.; Zhang, H. A Nano-Structured and Highly Ordered Polypyrrole-Sulfur Cathode for Lithium-Sulfur Batteries. *J. Power Sources* **2011**, *196*, 6951–6955.
26. Wu, F.; Wu, S.; Chen, R.; Chen, J.; Chen, S. Sulfur-Polythiophene Composite Cathode Materials for Rechargeable Lithium Batteries. *Electrochem. Solid-State Lett.* **2012**, *13*, A29–A31.
27. Yin, L.; Wang, J.; Yang, J.; Nuli, Y. A Novel Pyrolyzed Polyacrylonitrile-Sulfur@MWCNT Composite Cathode Material for High-Rate Rechargeable Lithium/Sulfur Batteries. *J. Mater. Chem.* **2011**, *21*, 6807–6810.
28. Li, W. Y.; Zheng, G. Y.; Yang, Y.; Seh, Z. W.; Liu, N.; Cui, Y. High-Performance Hollow Sulfur Nanostructured Battery Cathode through a Scalable, Room Temperature, One-Step, Bottom-Up Approach. *Proc. Natl. Acad. Sci. U.S.A.* **2013**, *110*, 7148–7153.
29. Ji, L. W.; Rao, M. M.; Zheng, H. M.; Zhang, L.; Li, Y. C.; Duan, W. H.; Guo, J. H.; Cairns, E. J.; Zhang, Y. G. Graphene Oxide as a Sulfur Immobilizer in High Performance Lithium/Sulfur Cells. *J. Am. Chem. Soc.* **2011**, *133*, 18522–18525.
30. Wang, H. L.; Yang, Y.; Liang, Y. Y.; Robinson, J. T.; Li, Y. G.; Jackson, A.; Cui, Y.; Dai, H. J. Graphene-Wrapped Sulfur Particles as a Rechargeable Lithium-Sulfur Battery Cathode Material with High Capacity and Cycling Stability. *Nano Lett.* **2011**, *11*, 2644–2647.
31. Kim, H.; Lim, H.-D.; Kim, K.; Kang, K. Graphene for Advanced Li/S and Li/air Batteries. *J. Mater. Chem. A* **2013** (Advance Article: DOI: 10.1039/C3TA12522J).
32. Evers, S.; Nazar, L. F. Graphene-Enveloped Sulfur in a One-Pot Reaction: A Cathode with Good Coulombic Efficiency and High Practical Sulfur Content. *Chem. Commun.* **2012**, *48*, 1233–1235.
33. Jayaprakash, N.; Shen, J.; Moganty, S. S.; Corona, A.; Archer, A. A. Porous Hollow Carbon@Sulfur Composites for High-Power Lithium-Sulfur Batteries. *Angew. Chem., Int. Ed.* **2011**, *50*, 5904–5908.
34. Kim, J.; Lee, D. J.; Jung, H. G.; Sun, Y. K.; Hassoun, J.; Scrosati, B. An Advanced Lithium-Sulfur Battery. *Adv. Funct. Mater.* **2012**, *23*, 1076–1080.
35. Zhang, C.; Wu, H. B.; Yuan, C.; Guo, Z.; Lou, X. W. Confining Sulfur in Double-Shelled Hollow Carbon Spheres for Lithium-Sulfur Batteries. *Angew. Chem., Int. Ed.* **2012**, *51*, 9592–9595.
36. Liu, J.; Qiao, S. Z.; Liu, H.; Chen, J.; Orpe, A.; Zhao, D.; Lu, G. Q. Extension of the Stöber Method to the Preparation of Monodisperse Resorcinol-Formaldehyde Resin Polymer and Carbon Spheres. *Angew. Chem., Int. Ed.* **2011**, *50*, 5947–5951.
37. Fuertes, A. B. Templated Synthesis of Mesoporous Carbons with a Controlled Particle Size. *J. Mater. Chem.* **2003**, *13*, 3085–3088.
38. Zhang, S. S. Role of $LiNO_3$ in Rechargeable Lithium/Sulfur Battery. *Electrochim. Acta* **2012**, *70*, 344–348.
39. Wang, J.; Kaskel, S. KOH Activation of Carbon-Based Materials for Energy Storage. *J. Mater. Chem.* **2012**, *22*, 23710–23725.
40. Bruno, M. M.; Cotella, N. G.; Miras, M. C.; Barbero, C. A. A Novel Way to Maintain Resorcinol-Formaldehyde Porosity during Drying: Stabilization of the Sol-Gel Nanostructure Using a Cationic Polyelectrolyte. *Colloids Surf., A: Physiochem. Eng. Aspects* **2010**, *362*, 28–32.
41. Hubbe, M. A.; Wu, N.; Rojas, O. J.; Park, S. Permeation of a Cationic Polyelectrolyte into Mesoporous Silica Part 3. Using Adsorption Isotherms to Elucidate Streaming Potential Results. *Colloids Surf., A: Physiochem. Eng. Aspects* **2011**, *381*, 1–6.
42. Park, M.-S.; Yu, J.-S.; Kim, K. J.; Jeong, G.; Kim, J.-H.; Yim, T.; Jo, Y.-N.; Hwang, U.; Kang, S.; Woo, T.; *et al*. Porous Carbon Spheres as a Functional Conducting Framework for Use in Lithium-Sulfur Batteries. *RSC Adv.* **2013**, *3*, 11774–11781.
43. Zhang, C.; Wu, H. B.; Yuan, C.; Guo, Z.; Lou, X. W. Confining Sulfur in Double-Shelled Hollow Carbon Spheres for Lithium-Sulfur Batteries. *Angew. Chem., Int. Ed.* **2012**, *51*, 9592–9595.
44. Zhang, K.; Zhao, Q.; Tao, Z.; Chen, J. Composite of Sulfur Impregnated in Porous Hollow Carbon Spheres as the Cathode of Li-S Batteries with High Performance. *Nano Res.* **2013**, *6*, 38–46.
45. Fuertes, A. B.; Valle-Vigón, P.; Sevilla, M. One-Step Synthesis of Silica@resorcinol-Formaldehyde Spheres and Their Application for the Fabrication of Polymer and Carbon Capsules. *Chem. Commun.* **2012**, *48*, 6124–6126.
46. Evers, S.; Yim, T.; Nazar, L. F. Understanding the Nature of Absorption/Adsorption in Nanoporous Polysulfide Sorbents for the Li-S Battery. *J. Phys. Chem. C* **2012**, *116*, 19653–19658.
47. Cuisinier, M.; Cabelguen, P.-E.; Evers, S.; He, G.; Kolbeck, M.; Garsuch, A.; Bolin, T.; Balasubramanian, M.; Nazar, L. F. Sulfur Speciation in Li−S Batteries Determined by Operando X-ray Absorption Spectroscopy. *J. Phys. Chem. Lett.* **2013**, *4*, 3227–3232.